

LASER PROCESSING OF HIGH-ENTROPY $\text{VNb}_2\text{TaCrMoWTi}_{0.3}\text{B}_{0.6}$ ALLOY COATINGS FOR WEAR REDUCTION IN DRY FRICTION WITH DIFFERENT COUNTERFACES

O.M. Myslyvchenko,^{1,4} R.V. Lytvyn,¹ K.E. Grinkevich,¹
O.B. Zgalat-Lozynskyy,¹ I.V. Tkachenko,¹ O.M. Bloschanevich,¹
S.E. Ivanchenko,¹ V.M. Novichenko,²
and O.P. Gaponova³

UDC 669.[017.15+058]:620.178.16

The microstructure, phase composition, and microhardness of the cast high-entropy $\text{VNb}_2\text{TaCrMoW}$ alloy with the addition of titanium diboride were studied. The initial $\text{VNb}_2\text{TaCrMoW}$ alloy consisted of two bcc solid solutions, slightly differing in lattice parameters ($a = 0.3139$ nm and 0.3200 nm). The addition of boron as titanium diboride and repeated remelting led to a bcc solid solution with a larger lattice parameter ($a = 0.3217$ nm) and a boride with $\text{W}_{3.5}\text{Fe}_{2.5}\text{B}_4$ structure ($a = 0.6054$ nm and $c = 0.3256$ nm). The bcc solid solution was the first to crystallize, and the boride was part of the eutectic grains and precipitated from the last melt portions, forming a closed network. The resulting alloy was applied to a carbon steel substrate as a coating using electrospark deposition employing an Elitron-24A installation with varying electrical pulse energy. Higher pulse energy during coating deposition increased the layer thickness and surface roughness but did not influence the phase composition. The microstructure of the coatings was more uniform compared to the cast alloys, and X-ray diffraction showed that the coatings contained bcc solid solutions, Fe_7W_6 intermetallic compound, and a small amount of TaO_2 oxide. The coatings had a hardness of about 10 GPa and were 11–15 μm and 16–20 μm thick at discharge energies of 0.52 and 1.1 J, respectively. A comparative analysis of the phase composition, hardness, and microstructure of the cast alloy and associated coatings was carried out. The coatings deposited at a discharge energy of 0.52 J were subjected to laser processing. Laser processing of the coatings resulted in a thermally affected zone, while the surface layer hardness hardly changed. The wear resistance of the coatings deposited at a discharge energy of 0.52 J was analyzed. Wear resistance testing was conducted for three counterface materials (VK6, Al_2O_3 , and Si_3N_4) in quasistatic and dynamic loading modes. Laser processing of the electrospark coatings changed the wear mechanism and significantly increased the wear resistance regardless of the counterface material and loading mode.

Keywords: high-entropy boride, electrospark deposition, solid solution, wear resistance, microstructure, X-ray diffraction.

¹Frantsevich Institute for Problems of Materials Science, National Academy of Sciences of Ukraine, Kyiv, Ukraine. ²Technical Center, National Academy of Science of Ukraine, Kyiv, Ukraine. ³Sumy State University, Sumy, Ukraine.

⁴To whom correspondence should be addressed; e-mail: zvyagina47@gmail.com.

Translated from Poroshkova Metallurgiya, Vol. 62, Nos. 5–6 (551), pp. 94–106, 2023. Original article submitted March 25, 2023.

INTRODUCTION

High-entropy alloys (HEAs) are not composed of a single element (metal) but a mixture of at least five elements, each present in nearly equiatomic concentrations. The V–Nb–Ta–Cr–Mo–W system is notable for the production of numerous HEAs, characterized by a disordered solid solution of a body-centered cubic (bcc) phase. The paper [1] shows that the cast equiatomic VNbTaCrMoW alloy demonstrates better compression performances from room temperature to 1600°C than many traditional creep-resistant alloys. Cast alloys in this system with a higher niobium content (VNb₂TaCrMoW) can be used as wear-resistant materials [2]. All the above studies were performed on cast alloys. However, the production of cast HEAs that are rich in expensive and scarce elements, such as niobium and tantalum, is costly. Consequently, the application of HEAs as protective coatings on more affordable steel substrates may be reasonable [3, 4]. Various methods exist for applying protective layers of required thickness and predefined properties. In our research, the electrospark deposition method was employed to produce the coatings.

Numerous studies have shown that the addition of boron to HEAs with a bcc structure strengthens the solid solution and leads to the formation of fine borides, in turn significantly enhancing the alloy [5, 6]. Therefore, boron was introduced in the form of titanium boride into the selected alloy composition, and the VNb₂TaCrMoWTi_{0.3}B_{0.6} HEA served as the electrode for applying ESD coatings.

The objective is to examine the effect of laser processing of VNb₂TaCrMoWTi_{0.3}B_{0.6} HEA coatings on the wear resistance in friction against VK6, Al₂O₃, and Si₃N₄ counterfaces.

EXPERIMENTAL PROCEDURE

The high-entropy VNb₂TaCrMoWTi_{0.3}B_{0.6} alloy was synthesized through arc melting from metals of more than 99.5 at.% purity and TiB₂ powder. The choice of boride instead of elemental boron was due to its significantly different density and melting point compared to other metallic constituents. The melting process was conducted with a nonconsumable tungsten electrode on a water-cooled copper hearth. The cooling rate was 80–100 K/sec. At the initial stage, the V, Nb, Ta, Cr, Mo, W, and Ti metals were melted in appropriate proportions in the arc furnace. The resultant ingots were mechanically ground into powder, and then TiB₂ powder was added to the mixture. The alloy underwent six remelting cycles to ensure uniform composition.

Electrospark coatings were applied to St3sp carbon steel substrates (0.14 : 0.22 C, 0.15 : 0.30 Si, 0.40 : 0.65 Mn, up to 0.3 Ni, up to 0.3 Cr, up to 0.05 S, up to 0.04 P), measuring 10 mm × 14 mm, employing an Elitron-24A installation. The coatings were applied in two stages: primary deposition at a single-discharge energy, W_d , of 0.52 J (coating 1) or 1.1 J (coating 2) and finishing deposition at a single-discharge energy of 0.24 J. Finishing deposition was intended to smooth out any micro-irregularities and reduce surface roughness [7].

The surface of coating 1 was subjected to laser processing (coating 1L) to homogenize the chemical composition and reduce porosity and internal stresses in the deposited layer. This laser processing was conducted using a Kvant-15 pulsed laser at a laser wavelength of 1.06 μm, pulse duration of 5 msec, focal length of 100 cm, pulse repetition rate of 10 Hz, spot diameter of 1.25 cm, voltage of 550 V, and pulse energy of 3.9 J. The coatings were deposited and laser-processed in air.

The phase composition of the cast alloys and the resulting coatings was analyzed by X-ray diffraction in the Bragg–Brentano focusing geometry employing a DRON-3 diffractometer in Co- K_α radiation.

Hardness testing and metallographic analysis were conducted on cross sections of the samples. The microstructure of the samples was examined on polished microsections with a JEOL JSM-6490LV scanning electron microscope, equipped with an INCAx-act analyzer from OXFORD Instruments. Hardness testing was performed with the Vickers method using a Buehler Micromet 2100 hardness testing machine in at least ten different fields of vision under a load of 0.098–0.49 N. The indenter was a diamond pyramid with a square base and a dihedral angle of 136° at the apex. The accuracy of the microhardness measurement was ±250 MPa.

The tribological properties of the samples were evaluated through dry friction tests using an ATKD automated tribological system [8] with a dynamic loading module, allowing a combination of quasistatic and

TABLE 1. Parameters of Friction Counterfaces for Tribological Tests of the Coatings

Counterface material	Hardness H_v , GPa	Elastic modulus, GPa	Density, g/cm ³
VK6	12.74–13.73	600	15.00
Al ₂ O ₃	16.67	350	3.87
Si ₃ N ₄	13.73–16.67	310	3.23

dynamic loads on a single friction track. The wear testing involved reciprocating sliding of a spherical counterface across the sample at a frequency of ~1 Hz with a friction track length of 8 mm. The tribological behavior was assessed for three counterfaces 8 mm in diameter from different materials (Table 1).

The quasistatic load was 30 N and was supplemented by a variable load component for dynamic testing, administered sinusoidally at a frequency of 25 Hz, with an amplitude of 3 N or 10% of the static load. The testing lasted 15 min (~1,000 cycles) at a sliding speed of 0.0147 m/sec at $T \approx 20^\circ\text{C}$.

The tribotechnical properties of the materials were subjected to rapid assessment in accordance with the procedure outlined in [9]. After each test, linear wear was quantified by measuring the surface profiles on the friction tracks using a Micron-Alpha noncontact interference profilometer in quasistatic and dynamic loading regions. Micron-Alpha was also used to determine the wear surface topography. The friction force during the tests was recorded with a sensor (inductive transducer) connected to an elastic component sensitive to displacements.

DISCUSSION OF RESULTS

The VNb₂TaCrMoW alloy consists of two solid solutions, both based on a bcc phase. These solutions slightly differ in lattice parameters (Fig. 1, Table 2). The addition of TiB₂ and subsequent remelting lead to the disappearance of the bcc₂ solid solution. This solution has a smaller lattice parameter and forms W₂CoB₂-type borides, with tungsten positions predominantly occupied by atoms with a larger atomic radius (Nb, Ta, Mo, W) and cobalt positions occupied by atoms with a smaller atomic radius (V, Cr).

Findings from scanning electron microscopy for the electrode used to apply coatings are illustrated in Fig. 2 and Table 3. According to X-ray diffraction, the VNb₂TaCrMoWTi_{0.3}B_{0.6} alloy consists of a solid solution (bcc₁) and W₂CoB₂ boride, with the bcc₁ phase being predominant (Table 2). The light region (dendrite) is attributed to the bcc₁ phase, while the gray one to the W₂CoB₂ boride. In this alloy, the boride crystallizes eutectically (Fig. 2) from the last melt portions, forming a closed network. Local chemical analysis (Table 3) indicates that boron is absent in the solid solution. However, note that the boron concentration was measured tentatively in our research, as

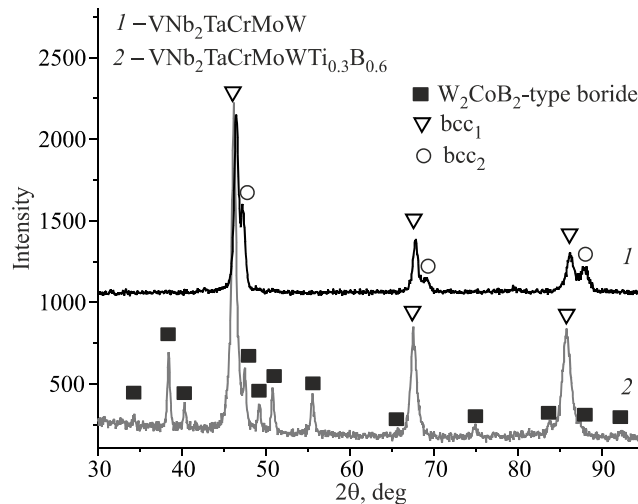


Fig. 1. XRD results for the alloys

TABLE 2. Phase Composition and Lattice Parameters of the Alloys

Alloy	Phase composition		Lattice parameters, nm
	Structure	vol.%	
VNb ₂ TaCrMoW	bcc ₁	42	<i>a</i> = 0.3200
	bcc ₂	58	<i>a</i> = 0.3139
VNb ₂ TaCrMoWTi _{0.3} B _{0.6}	bcc ₁	65	<i>a</i> = 0.3217
	W ₂ CoB ₂	35	<i>a</i> = 0.6054 <i>c</i> = 0.3256

TABLE 3. Local Chemical Composition (at.%) of the Cast VNb₂TaCrMoWTi_{0.3}B_{0.6} HEA and Electron Concentration of Phase Constituents

Structure	V	Nb	Ta	Cr	Mo	W	Ti	B	HEA, e/a
bcc ₁	9.2	28.2	17.9	1.3	19.0	22.2	2.2	–	5.4
W ₂ CoB ₂	9.3	18.3	8.0	6.0	6.5	4.1	2.4	45.4	4.2

boron has a small atomic mass and thus its characteristic lines are difficult to detect in the spectrum. Boron probably not only formed the boride but also partially dissolved in the bcc₁ lattice. The high entropy of the alloy promotes higher mutual solubility of the elements, allowing the boron content to reach 4 at.% in the HEA bcc solid solutions [6]. The greater bcc₁ lattice parameters after TiB₂ is added to the VNb₂TaCrMoW alloy and the microhardness of the material are also indicative of boron being present in the solid solution (Table 2). Microindentation data show that the hardness of the eutectic in the VNb₂TaCrMoWTi_{0.3}B_{0.6} alloy is 10 GPa and that of the bcc₁ solid solution is 7 GPa, while the microhardness of the VNb₂TaCrMoW alloy is 5–6 GPa.

The mixing enthalpy for B–V, B–Nb, B–Ta, B–Cr, B–Mo, and B–W is –42, –54, –54, –31, –34, and –31 kJ/mol, respectively [10]. The significant negative mixing enthalpy underscores the strong bonding between the B–V, B–Nb, and B–Ta atomic pairs. This explains why V, Nb, and Ta elements are predominant in the boride (Table 3). Note also that the average electron concentration of the boride is much lower than that of the bcc phase as boron has only three electrons in its outer energy level.

The electrodes were made from the ingots through electrospark cutting and grinding, and the electrospark coatings were deposited at varying discharge energy.

Figure 3 illustrates the relationship between the sample’s weight increment and the coating deposition time. The use of a higher single-pulse energy (1.1 J) results in a more significant mass transfer from the electrode to the

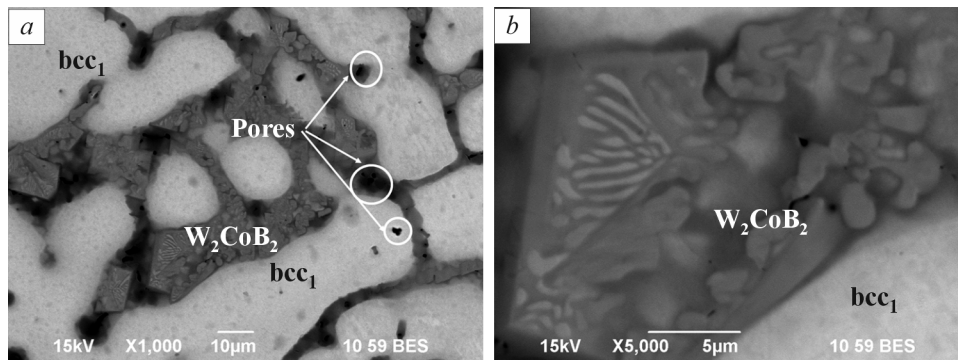


Fig. 2. SEM image of the VNb₂TaCrMoWB_{0.6} alloy in backscattered electrons

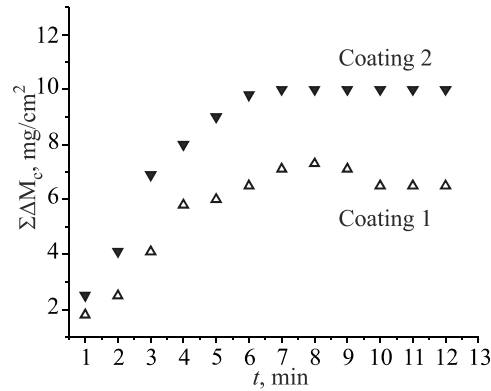


Fig. 3. Kinetic dependences for the cathode weight increment in the deposition of coatings with the $\text{VNb}_2\text{TaCrMoWB}_{0.6}$ electrode

TABLE 4. Thickness of the $\text{VNb}_2\text{TaCrMoWTi}_{0.3}\text{B}_{0.6}$ ESD Coatings and Their Microhardness at a Distance of 5 μm from the Surface

Coating	Discharge energy, J	Layer thickness, μm	Microhardness, MPa
1	0.52	11–15	10
2	1.1	16–20	10
1L	0.52 + laser	11–15	10–11

substrate. The cathode weight increment is observed when the deposition process lasts 7–8 min. During further processing, the coating weight remains unchanged and even decreases at a single-pulse energy of 0.52 J. This is due to the accumulation of defects and stresses in the applied layer, leading to its degradation under the action of electrospark pulses. Table 4 presents data on the thickness and hardness of the coatings. Changes in the discharge energy in the deposition process have no effect on the hardness but increase thickness of the coatings. The microhardness of the interface between the ESD coating and the substrate is 3–3.5 GPa, while the substrate microhardness is 1.7–1.9 GPa. Note also that laser processing increases the microhardness at the coating–substrate interface to 6–7 GPa.

Figure 4 shows the cross-sectional microstructure of coating 1 and the distribution of some elements in it. Noteworthy is that iron penetrates into the coating as the substrate metal is mixed with the electrode (Fig. 4c). There are no defects or a transition layer at the coating–substrate interface. The microstructure of the coating is homogeneous (single-phase) and does not resemble the microstructure of the electrode for applying the coating. In this regard, the phase composition of the coatings is of great interest. Figure 5 indicates that the coating is not single-phase, consisting primarily of Fe_7W_6 intermetallic compound and a bcc solid solution with lattice parameter $a = 0.3030$ nm. Since there was no protective atmosphere in the coating deposition process, oxides of TaO_2 type formed. These three phase constituents are probably ultrafine and uniformly distributed over the coating cross-section, and thus invisible in the microstructure. Additional laser processing increased the TaO_2 content in the coating material, while the lattice parameter of the bcc solid solution decreased to 0.2880 nm.

Increase in the discharge energy to 1.1 J did not lead to changes in the phase composition, but surface roughness increased significantly and fused spots and micro-irregularities formed on the surface, which remained unaffected by finishing processing at a discharge energy of 0.24 J. These coating relief features significantly reduce the reproducibility of tribological test results in terms of wear and, especially, friction force [11]. In this regard, coating 1 deposited at a discharge energy of 0.52 J was chosen for tribological tests. The wear patterns were analyzed for different indenters under different loading modes. The friction and wear tests resulted in friction tracks (Fig. 6) for determining the wear parameters.

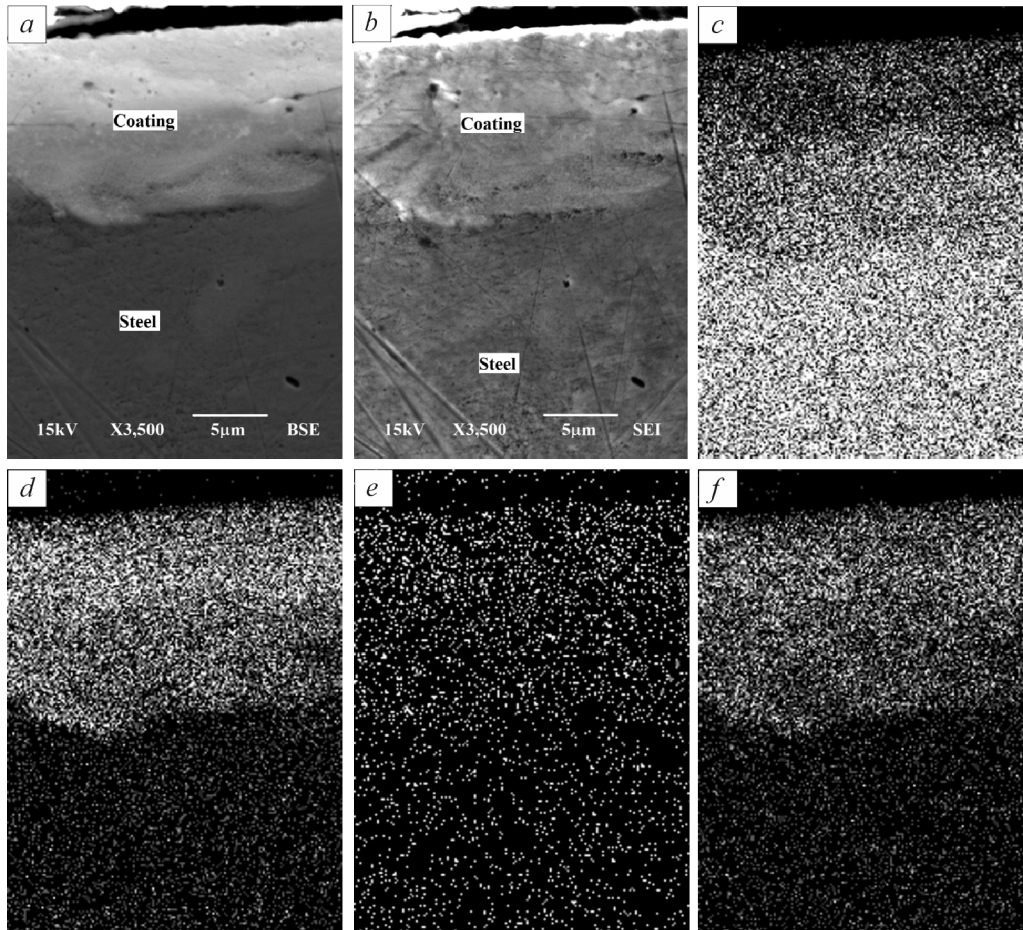


Fig. 4. Microstructure of coating 1 (discharge energy of 0.52 J) in backscattered (a) and secondary (b) electrons and in characteristic radiation of Fe- K_{α} (c), W- K_{α} (d), Ta- K_{α} (e), and Nb- K_{α} (f)

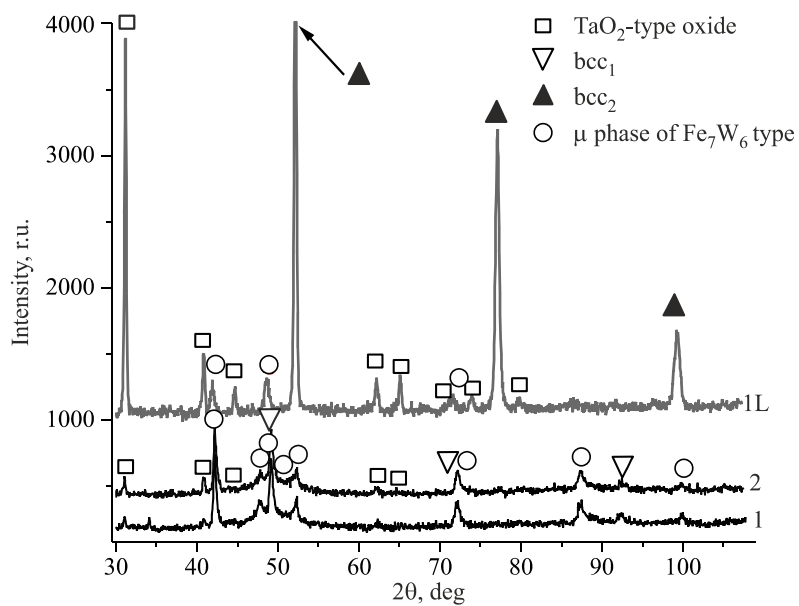


Fig. 5. X-ray diffraction patterns for the $\text{VNb}_2\text{TaCrMoWTi}_{0.3}\text{B}_{0.6}$ coatings deposited at a discharge energy of 0.52 J (coatings 1 and 1L) and 1.1 J (coating 2)

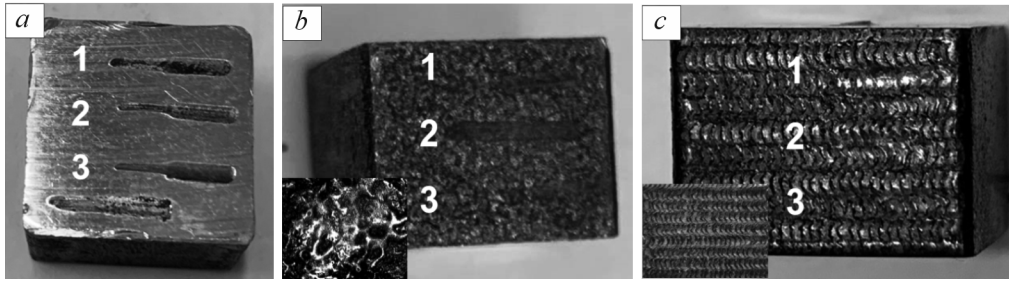


Fig. 6. Surface of the St3sp steel samples in the starting state (a), with coating 1 (b), and with coating 1L (c) after friction tests with the Si_3N_4 (1), Al_2O_3 (2), and VK6 (3) indenters

As a result of friction and wear tests, friction tracks were recorded (Fig. 6) for determining wear parameters. The surface of the friction tracks is shown in Fig. 6.

The wear and friction indicators determined in quasistatic and dynamic loading modes are presented in Fig. 7. Wear observed in the dynamic mode is greater than wear in the quasistatic mode for both uncoated and coated steel. The contribution of the dynamic component to wear intensification increases in the following sequence of indenters: $\text{Si}_3\text{N}_4 \rightarrow \text{Al}_2\text{O}_3 \rightarrow \text{VK6}$. The ESD coating tested with the Al_2O_3 counterface exhibited the least sensitivity to load variations. This phenomenon may be attributed to the lowest friction force between the coating material and the Al_2O_3 indenter. In all tests, except for coating 1 with the Al_2O_3 counterface, the uncoated surface showed more significant wear than the coated surfaces under the quasistatic conditions (Fig. 7a). Note that the CoCrFeNiMn HEA also demonstrated the least wear resistance with the Al_2O_3 indenter in [12]. The lowest wear under both loading conditions was recorded for the laser-processed coating (1L). This sample showed almost no

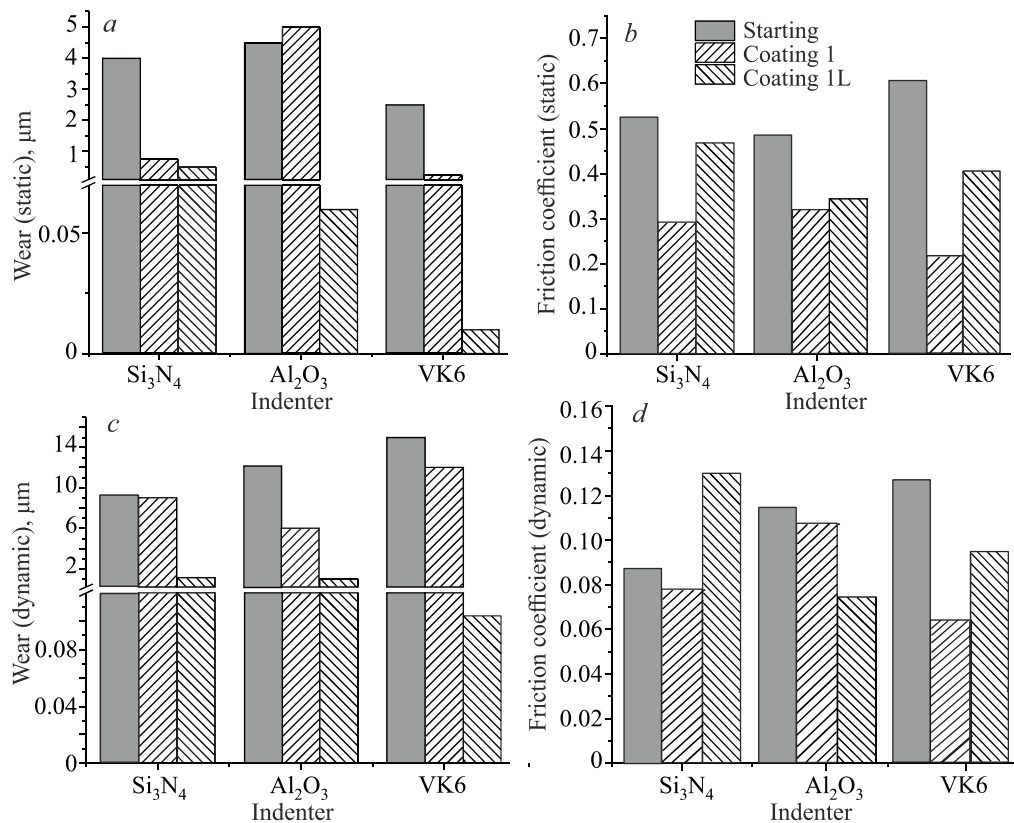


Fig. 7. Wear (a, c) and friction coefficient (b, d) of the samples under static (a, b) and dynamic (c, d) loads

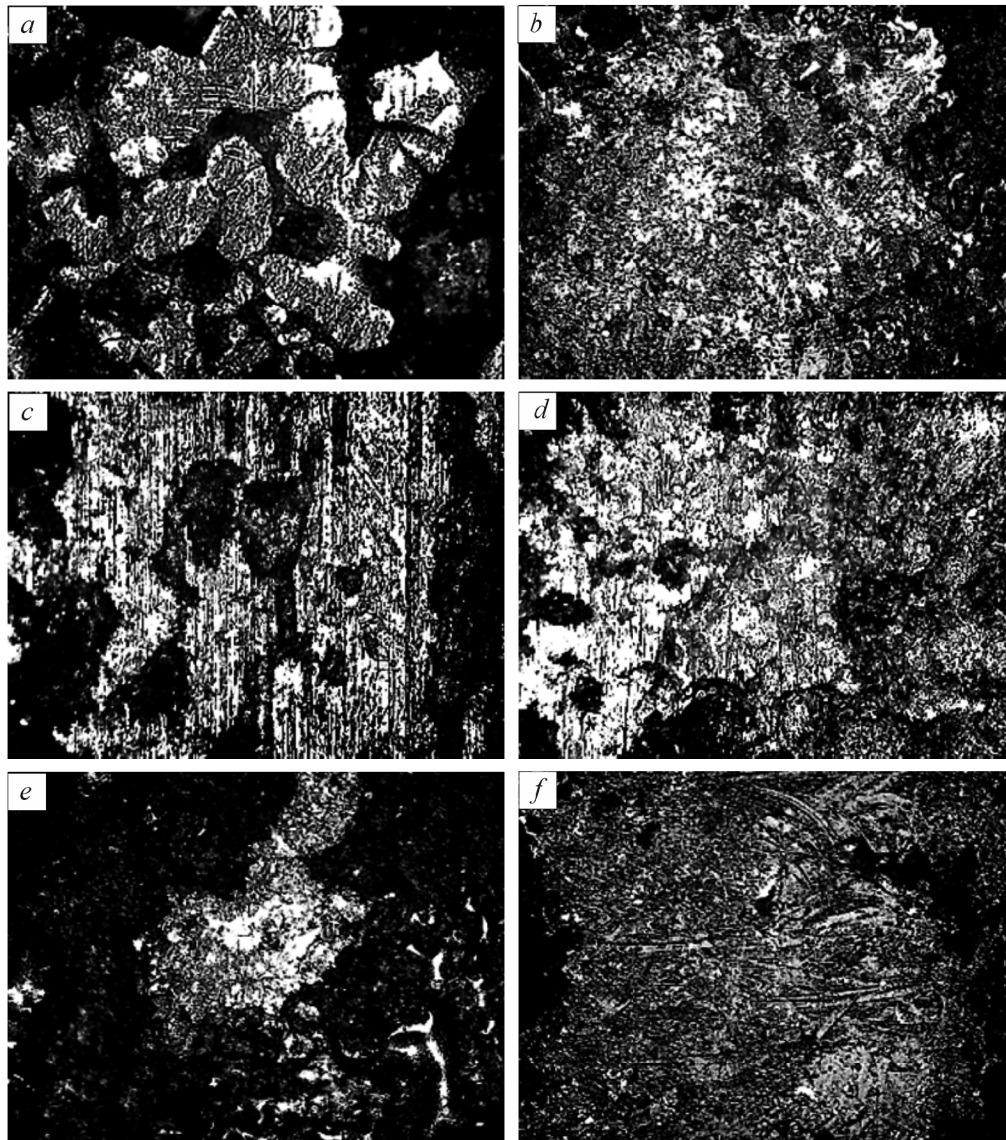


Fig. 8. Morphology of the friction surfaces of coating 1 under quasistatic (*a, c, e*) and dynamic (*b, d, f*) loads tested with the Si_3N_4 (*a, b*), Al_2O_3 (*c, d*), and VK6 (*e, f*) indenters

wear signs in both dynamic and quasistatic modes across all indenters. The distinctive surface texture resulting from laser processing was largely preserved after friction testing.

The friction coefficient (μ) of various indenters on uncoated steel increases in the following sequence: $\text{Al}_2\text{O}_3 \rightarrow \text{Si}_3\text{N}_4 \rightarrow \text{VK6}$ as $0.48 \rightarrow 0.54 \rightarrow 0.6$. These high μ values are characteristic of steel–ceramic friction pairs in the absence of lubrication. High friction coefficients are also observed in steel–HEA pairs. It is reported that μ can reach unity for some high-entropy alloys [13]. In our experiments, the application of HEA coatings, depending on the surface relief and compatibility with the counterface, leads to a one-third to two-third reduction in the friction coefficient compared to the uncoated substrate (Fig. 7*b, d*).

The surface relief of the coatings is a key factor influencing the surface friction coefficient, regardless of the counterface material. Laser processing enhances the surface relief compared to coating 1 (Fig. 6*b, c*), resulting in increased friction for all indenters, except for the Al_2O_3 indenter under dynamic loading. The wear mechanism of the coatings changes after laser processing (coatings 1 and 1L), as evidenced by the morphology of the friction surfaces (Figs. 8 and 9). The influence of the indenter material on the friction surface morphology was found to be more pronounced for coating 1.

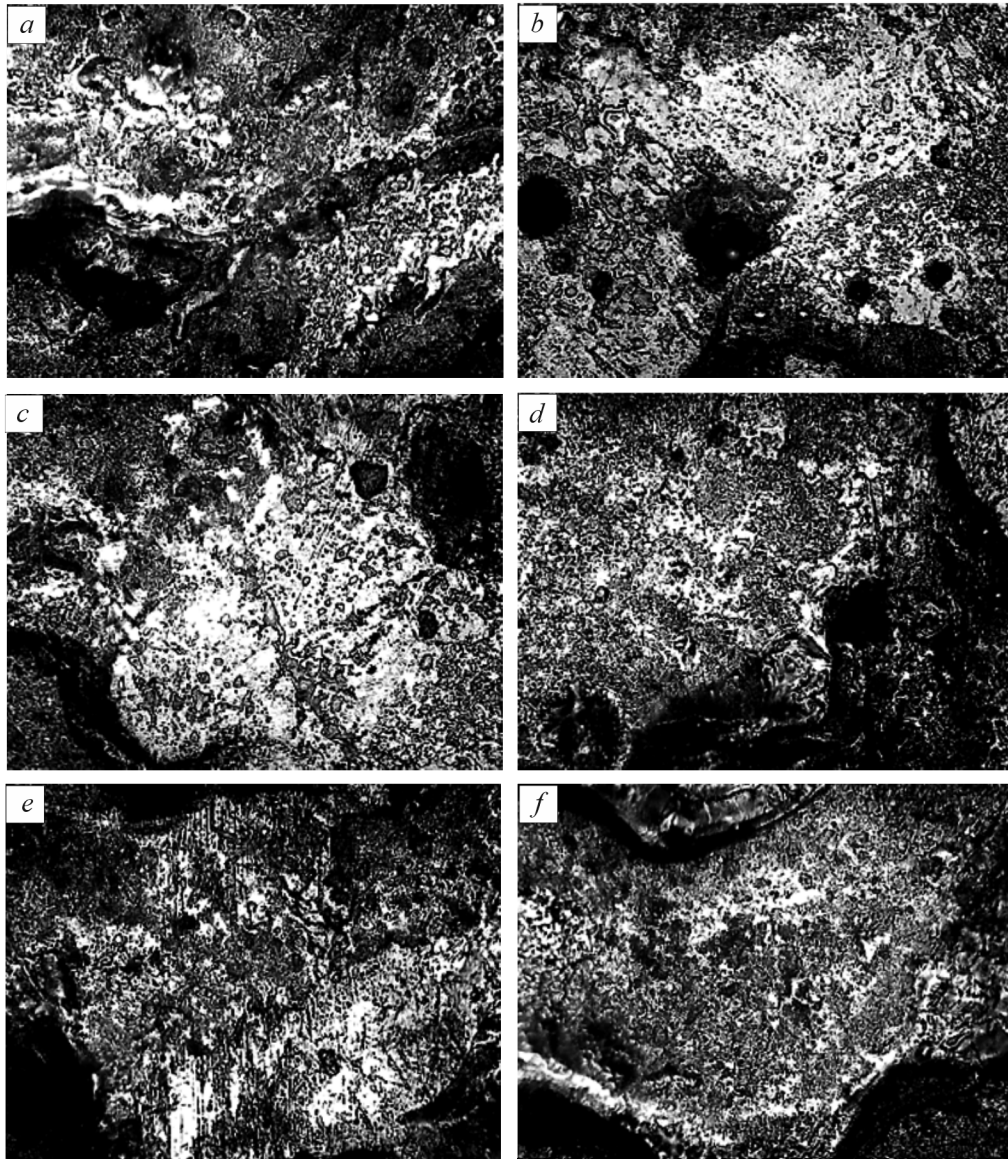


Fig. 9. Morphology of the friction surfaces of coating 1L under quasistatic (*a, c, e*) and dynamic (*b, d, f*) loads tested with the Si_3N_4 (*a, b*), Al_2O_3 (*c, d*), and VK6 (*e, f*) indenters

The images of friction tracks for coating 1 under quasistatic loading show grooves and white deposits, being indicative of abrasive wear, and dark spots, being indicative of partial adhesive surface interaction. In the coating 1– Al_2O_3 counterface pair, the friction surfaces in both loading modes are similar, particularly in terms of adhesive wear indicators. This similarly supports the predominant role of a single wear mechanism and aligns with the findings that highlight the minimal impact of the dynamic component on the wear resistance of this friction pair. For coating 1L, there is an insignificant difference in the surface morphology of the friction tracks between quasistatic and dynamic loads across all indenters.

The white regions on the friction surfaces of coating 1L in both loading modes are likely oxidized layers formed atop micro-irregularities (Fig. 9). Although coating 1L exhibited a slightly higher friction coefficient compared to coating 1, there were no evident signs of adhesive wear or destruction of ridges in its friction interactions. Wear was virtually absent for all indenters used with coating 1L. The absence of wear debris along the friction tracks of coating 1L may also suggest that the wear mechanism is primarily oxidative rather than abrasive or adhesive and that there is a good compatibility between the coating and counterface. Note that coating 1L

demonstrates high wear resistance, especially in dynamic loading conditions, closely resembling actual operating environments. The highest wear resistance under all loading conditions was observed for laser-processed coating 1L tested with the VK6 hardmetal indenter.

CONCLUSIONS

Coatings from the $\text{VNb}_2\text{TaCrMoWB}_{0.6}$ HEA have been applied to St3sp substrates by ESD. The coatings are distinguished by high integrity and low porosity. Contrastingly to the cast state, the microstructure of the HEA coatings is more uniform and free from boride-phase inclusions.

The phase compositions of cast HEAs and their resultant coatings differ. The cast $\text{VNb}_2\text{TaCrMoWB}_{0.6}$ alloy contains solid solutions and borides. Coatings from this alloy consist of solid solutions, Fe_7W_6 intermetallic compound, and TaO_2 -type oxide. When ESD coatings from the $\text{VNb}_2\text{TaCrMoWB}_{0.6}$ alloy are applied without a protective atmosphere, TaO_2 -type oxide is formed, whose amount further increases during laser processing of the coating in air. To produce $\text{VNb}_2\text{TaCrMoWB}_{0.6}$ alloy coatings without oxide phases, a protective atmosphere should be employed during both coating deposition and subsequent laser processing.

Electrospark deposited coatings double the wear resistance of the samples when tested with the Al_2O_3 indenter under the dynamic loading mode and increase the wear resistance tenfold with the VK6 indenter under the quasistatic loading mode.

Laser processing has a negligible impact on the hardness of the coatings. However, the wear resistance of the laser-processed coatings has increased by 25 times under quasistatic loading and 100 times under dynamic loading with the VK6 indenter. The HEA coatings have significantly reduced the friction coefficient, from one-third to two-thirds, depending on the surface relief and compatibility with the indenters. Besides the compatibility between the laser-processed coating and the indenter, this effect can also be attributed to change in the wear mechanism from abrasive + adhesive to predominantly oxidative.

The comparative tests have demonstrated the effectiveness of $\text{VNb}_2\text{TaCrMoWB}_{0.6}$ HEA coatings (under different ESD and laser processing conditions) in enhancing the wear resistance of tribological components. These coatings show substantial wear resistance under severe loading conditions.

REFERENCES

1. O.N. Senkov, G.B. Wilks, J.M. Scott, and D.B. Miracle, "Mechanical properties of $\text{Nb}_{25}\text{Mo}_{25}\text{Ta}_{25}\text{W}_{25}$ and $\text{V}_{20}\text{Nb}_{20}\text{Mo}_{20}\text{Ta}_{20}\text{W}_{20}$ refractory high entropy alloys," *Intermetallics*, **19**, No. 5, 698–706 (2011).
2. S.A. Firstov, V.F. Gorban, N.A. Krapivka, and E.P. Pechkovskii, "New class of materials—high-entropy alloys and coatings," *Vest. Ros. Univ. Mat.*, **18**, 1938–1940 (2013).
3. A.I. Yurkova, D.V. Hushchyk, and A.V. Minitsky, "Synthesis of high-entropy AlNiCoFeCrTi coating by cold spraying," *Powder Metall. Met. Ceram.*, **59**, No. 11–12, 681–694 (2021).
4. D.V. Hushchyk, A.I. Yurkova, V.V. Cherniavsky, I.I. Bilyk, and S.O. Nakonechnyy, "Nanostructured AlNiCoFeCrTi high-entropy coating performed by cold spray," *Appl. Nanosci.*, **10**, 4879–4890 (2020).
5. X. Gao, L. Wang, N. Guo, L. Luo, G. Zhu, C. Shi, and J. Guo, "In-situ development of MB_2 and their effect on microstructure and mechanical properties of refractory $\text{Hf}_{0.5}\text{Mo}_{0.5}\text{NbTiZr}$ high entropy alloy matrix composites," *Int. J. Refract. Met. Hard Mater.*, **96**, 105473 (2021).
6. H. Zhang, H. Tang, Y.Z. He, J.L. Zhang, W.H. Li, and S. Guo, "Effect of heat treatment on borides precipitation and mechanical properties of $\text{CoCrFeNiAl}_{1.8}\text{Cu}_{0.7}\text{B}_{0.3}\text{Si}_{0.1}$ high-entropy alloy prepared by arc-melting and laser-cladding," *JOM*, **69**, No. 11, 2078–2083 (2017).
7. O.M. Myslyvhenko, O.P. Gaponova, V.B. Tarelynyk, and M.O. Krapivka, "The structure formation and hardness of high-entropy alloy coatings obtained by electrospark deposition," *Powder Metall. Met. Ceram.*, **59**, No. 3–4, 201–208 (2020).

8. Yu.V. Milman, K.E. Grinkevich, I.V. Tkachenko, V.Kh. Melnyk, and O.I. Lukyanov, *Method for Rapid Assessment of Tribotechnical Properties of Materials at Low Temperatures* [in Ukrainian], Utility Patent 127730, Application No. 201712397 dated December 14, 2017; publ. August 27 (2018), Bulletin No. 16.
9. J. Wang, H. Li, K. Grinkevych, R. Huang, J. Xu, G. Tsybanov, and I. Tkachenko, "Cyclic indentation method applied to evaluating surface degradation of cylinder-piston group parts," *Strength Mater.*, No. 5, 1–9 (2021).
10. A. Takeuchi and A. Inoue, "Classification of bulk metallic glasses by atomic size difference, heat of mixing and period of constituent elements and its application to characterization of the main alloying element," *Mater. Trans.*, **46**, No. 12, 2817–2829 (2005).
11. S. Pham-Ba and J.F. Molinari, "Creation and evolution of roughness on silica under unlubricated wear," *Wear*, **472**, 203648 (2021).
12. M. Zhang, Z. Jiang, M. Niu, Y. Sun, and X. Zhang, "Tribological behavior of CoCrFeNiMn high-entropy alloy against 304, Al₂O₃ and Si₃N₄ counterparts," *Wear*, **508**, 204471 (2022).
13. C.Y. Hsu, T.S. Sheu, J.W. Yeh, and S.K. Chen, "Effect of iron content on wear behavior of AlCoCrFe_xMo_{0.5}Ni high-entropy alloys," *Wear*, **268**, No. 5–6, 653–659 (2010).